

# Dominance of collective over proton transfer couplings in the fusion of $^{32}\text{S}$ and $^{34}\text{S}$ with $^{89}\text{Y}$

A. Mukherjee,<sup>1</sup> M. Dasgupta,<sup>1</sup> D. J. Hinde,<sup>1</sup> K. Hagino,<sup>2</sup> J. R. Leigh,<sup>1</sup> J. C. Mein,<sup>1</sup> C. R. Morton,<sup>1</sup> J. O. Newton,<sup>1</sup> and H. Timmers<sup>1,3</sup>

<sup>1</sup>*Department of Nuclear Physics, Research School of Physical Sciences and Engineering, Australian National University, Canberra ACT 0200, Australia*

<sup>2</sup>*Yukawa Institute for Theoretical Physics, Kyoto University, Kyoto 606-8502, Japan*

<sup>3</sup>*School of Physics, University of New South Wales at the Australian Defence Force Academy, Canberra ACT 2600, Australia*

(Received 17 June 2002; published 11 September 2002)

Fusion excitation functions have been measured to high precision for the reactions  $^{32}\text{S}+^{89}\text{Y}$  and  $^{34}\text{S}+^{89}\text{Y}$ . The sub-barrier fusion cross sections for  $^{32}\text{S}+^{89}\text{Y}$  are found to be more enhanced over single-barrier penetration calculations than those for  $^{34}\text{S}+^{89}\text{Y}$ , and the shapes of the two experimental barrier distributions are significantly different. The effects of proton transfer and double phonon excitations have been examined using exact coupled channels calculations. These suggest that the difference between the two systems lies mainly in the collectivity of the projectiles, whilst proton transfer has only a minor effect.

DOI: 10.1103/PhysRevC.66.034607

PACS number(s): 25.70.Jj, 24.10.Eq

## I. INTRODUCTION

Fusion of heavy nuclei at energies around the Coulomb barrier has been studied extensively [1–4], yet there are dynamical aspects that are not fully understood. It is well recognized that the fusion process is strongly influenced by the internal degrees of freedom of the colliding nuclei, such as rotation, vibration, and transfer of nucleons between the interacting nuclei. The coupling of the relative motion to these degrees of freedom leads to an enhancement of the fusion cross sections at energies below the average fusion barrier, relative to the cross sections expected from the single-barrier penetration model. It has been shown [5] that in the eigenchannel approximation, the effect of channel couplings is to replace the single fusion barrier by a distribution of barriers of different heights, some of which are lower than the height of the single (uncoupled) barrier. This qualitatively explained the observed enhancement [1,2] of experimental cross sections at sub-barrier energies. However, the nature of the couplings affecting the fusion process was not always apparent from the measured fusion cross sections. It was proposed by Rowley *et al.* [6] that a barrier distribution, resulting from channel couplings, could be extracted from a precisely measured fusion excitation function. Leigh *et al.* [7] demonstrated the success of this approach, which allows a deeper insight into the dynamics of fusion. Subsequently, this approach has been used extensively to understand the fusion mechanism in a wide range of reactions [4], usually dominated by vibrational and/or rotational couplings.

The effect of couplings to transfer channels has however, been studied for relatively few systems, notably  $^{16,17}\text{O}+^{144}\text{Sm}$  [8],  $^{32,36}\text{S}+^{110}\text{Pd}$  [9],  $^{40}\text{Ca}+^{90,96}\text{Zr}$  [10], and  $^{40}\text{Ca}+^{46,48,50}\text{Ti}$  [11]. These measurements showed that couplings to positive  $Q$ -value neutron transfer channels lead to a substantial enhancement in sub-barrier fusion cross sections. However, very few measurements [12,13] exist where the effect of proton transfer on the fusion process has been investigated.

In this work, fusion excitation functions have been measured precisely for the two systems,  $^{32}\text{S}+^{89}\text{Y}$  and  $^{34}\text{S}$

+ $^{89}\text{Y}$ , in order to investigate the effect of positive  $Q$ -value proton transfers on the fusion cross sections and barrier distributions. Unlike neutron transfer, for charged particle transfer, there is a change in the Coulomb energy which must be taken into account. Thus instead of the  $Q$ -value appropriate for transfer at infinite separation, an effective  $Q$ -value  $Q_{\text{eff}}$  is used. This  $Q_{\text{eff}}$  is defined as  $Q+\Delta V_C$ , where  $\Delta V_C$  is the change in the Coulomb energy at the fusion barrier radius resulting from the transfer. The values of  $Q_{\text{eff}}$  for various transfers leading to the ground states are listed in Table I for the two reactions  $^{32,34}\text{S}+^{89}\text{Y}$ . For  $^{32}\text{S}+^{89}\text{Y}$ , the transfer channels with positive values of  $Q_{\text{eff}}$  are single proton stripping with  $Q_{\text{eff}}=+2.635$  MeV, and two proton stripping with  $Q_{\text{eff}}=+3.900$  MeV. In contrast, for  $^{34}\text{S}+^{89}\text{Y}$ , only the single proton stripping has a positive value of  $Q_{\text{eff}}=+0.589$  MeV.

Besides the difference in the transfer  $Q$  values, the projectiles also differ structurally. The nuclei  $^{32}\text{S}$  and  $^{34}\text{S}$  are located in the  $sd$  shell and have eight-nucleon and six-nucleon holes, respectively, in the  $N=Z$  double closed shell. Both exhibit collective behavior, with electric quadrupole ( $E2$ ) transition strengths from the  $2_1^+$  states to ground states of  $^{32}\text{S}$  and  $^{34}\text{S}$  being 10.1 [14] and 6.4 [15] Weisskopf units, respectively. The nucleus  $^{32}\text{S}$  has a reasonably close multip-

TABLE I. Effective  $Q$ -values  $Q_{\text{eff}}$  for various transfer channels for the reactions  $^{32,34}\text{S}+^{89}\text{Y}$ .

Channel	$Q_{\text{eff}}$ (MeV)	
	$^{32}\text{S}+^{89}\text{Y}$	$^{34}\text{S}+^{89}\text{Y}$
$n$ pickup	−2.837	−4.493
$n$ stripping	−8.185	−4.560
$p$ pickup	−7.677	−3.559
$p$ stripping	+2.635	+0.589
$2n$ pickup	−0.771	−3.955
$2n$ stripping	−13.305	−5.268
$2p$ pickup	−16.243	−8.261
$2p$ stripping	+3.900	−0.425

let of  $0^+$ ,  $2^+$ , and  $4^+$  levels at approximately twice the energy of the  $2_1^+$  state as might be expected for a two-phonon state if  $^{32}\text{S}$  behaved as a near-harmonic vibrator. The strengths of the  $E2$  transitions from the members of this multiplet to the  $2_1^+$  state are also collective, for example, 11.9 W.u. (Weisskopf unit) [14] for the transition  $4_1^+ \rightarrow 2_1^+$ , supporting the vibrational picture. The nucleus  $^{34}\text{S}$  also has a similar multiplet, though the strengths of the  $E2$  transitions from them to the  $2_1^+$  state are smaller [15] than for  $^{32}\text{S}$ , thus indicating that  $^{34}\text{S}$  is less collective than  $^{32}\text{S}$ . In addition, in  $^{34}\text{S}$ , a  $1^+$  and a  $2^+$  state also appear in the vicinity of the multiplet, which have been identified [15] as single-particle states. It has been suggested [15] that mixing of single-particle states with collective vibrations occurs in  $^{34}\text{S}$ . It is unlikely that nuclei such as  $^{32}\text{S}$  and  $^{34}\text{S}$ , with such a small number of nucleon holes, could behave as harmonic vibrators, and  $^{36}\text{S}$  with no neutron holes appears as a typical closed shell nucleus with low collectivity. The  $2_1^+$  states in both  $^{32}\text{S}$  and  $^{34}\text{S}$  have finite values of quadrupole moments [16], which argues against them being spherical vibrators. However, it is clear that  $^{32}\text{S}$  is more collective than  $^{34}\text{S}$  and might therefore be better approximated as a harmonic vibrator. It is therefore interesting to see whether the present measurements will reflect the expected structural difference between  $^{32}\text{S}$  and  $^{34}\text{S}$ .

## II. EXPERIMENTAL PROCEDURE

The 14UD Pelletron accelerator at the Australian National University provided pulsed  $^{32,34}\text{S}$  beams ( $\approx 1$  ns wide beam bursts separated by 530 ns). The measurements were carried out with beam energies  $E_{\text{beam}}$  in the range 99.0–124.0 MeV, as listed in Table II. The target was  $^{89}\text{Y}$  of thickness  $\approx 40 \mu\text{g}/\text{cm}^2$  evaporated onto a  $\approx 10 \mu\text{g}/\text{cm}^2$  C backing, downstream of  $^{89}\text{Y}$ .

Fusion evaporation residues (ERs) were detected using a compact velocity filter [17] and a hybrid detector. The latter consisted of a position-sensitive, multiwire, gas proportional detector backed with a stopping position-sensitive silicon surface barrier (SSB) detector. The velocity filter transmitted the ERs to the detector whilst deflecting the intense elastically scattered beam particles to one side, where they were intercepted by a movable tantalum finger. With this arrangement, the ERs could be precisely measured at angles as small as  $1^\circ$  with respect to the beam axis. The ERs were identified by the energy deposited in the SSB detector and the time of flight (TOF) relative to the pulsed beam. Figures 1(a) and 1(b) show two typical spectra for the energy  $E$  deposited in the position-sensitive SSB detector vs TOF, at  $E_{\text{beam}} = 108.0$  and  $124.0$  MeV, for the reaction  $^{32}\text{S} + ^{89}\text{Y}$ . At larger scattering angles, where the elastic scattering yields were relatively small, the ERs were detected and identified by their energy and TOF using a SSB detector, having 11.9 times the solid angle of the velocity filter. This detector was mounted on the same movable arm as the velocity filter but displaced from it by a nominal angle of  $20^\circ$ . It allowed direct observation of ERs at angles  $> 10^\circ$ . Full angular distributions of the ERs were measured at  $E_{\text{beam}} = 106.0, 109.0,$

TABLE II. Fusion cross sections for  $^{32,34}\text{S} + ^{89}\text{Y}$  measured in this work; quoted errors are statistical uncertainties only. The c.m. energies are the values after correcting for energy loss in the target.

$E_{\text{beam}}$ (MeV)	$^{32}\text{S} + ^{89}\text{Y}$		$^{34}\text{S} + ^{89}\text{Y}$	
	$E_{\text{c.m.}}$ (MeV)	$\sigma_{\text{fus}}$ (mb)	$E_{\text{c.m.}}$ (MeV)	$\sigma_{\text{fus}}$ (mb)
99.00	72.68	$0.06 \pm 0.02$		
100.00	73.42	$0.50 \pm 0.07$	72.23	$0.03 \pm 0.02$
101.00	74.16	$1.7 \pm 0.1$	72.95	$0.18 \pm 0.02$
102.00	74.89	$4.6 \pm 0.2$	73.67	$0.73 \pm 0.06$
103.00	75.63	$10.7 \pm 0.3$	74.40	$3.0 \pm 0.1$
104.00	76.36	$19.6 \pm 0.3$	75.12	$8.8 \pm 0.2$
105.00	77.17	$33.6 \pm 0.4$	75.84	$19.9 \pm 0.4$
106.00 <sup>a</sup>	77.83	$47.9 \pm 0.5$	76.57	$35.2 \pm 0.5$
107.00	78.57	$66.4 \pm 0.7$	77.29	$53.6 \pm 0.5$
107.50			77.66	$63.3 \pm 0.6$
108.00	79.30	$86.2 \pm 0.9$	78.02	$75.5 \pm 0.8$
108.50			78.38	$85.3 \pm 0.8$
109.00 <sup>a</sup>	80.00	$109 \pm 1$	78.74	$97.8 \pm 1.0$
109.50			79.10	$107 \pm 1$
110.00	80.78	$132 \pm 1$	79.46	$121 \pm 1$
110.50			79.82	$132 \pm 1$
111.00	81.51	$157 \pm 2$	80.18	$146 \pm 1$
111.50			80.55	$159 \pm 1$
112.00 <sup>a</sup>	82.25	$183 \pm 2$	80.93	$172 \pm 2$
112.50			81.27	$183 \pm 2$
113.00	82.98	$205 \pm 2$	81.63	$196 \pm 2$
113.50			82.00	$208 \pm 2$
114.00	83.72	$234 \pm 2$	82.36	$223 \pm 2$
114.50			82.72	$238 \pm 2$
115.00	84.46	$261 \pm 3$	83.08	$246 \pm 2$
115.50			83.44	$262 \pm 3$
116.00	85.20	$282 \pm 3$	83.80	$273 \pm 3$
117.00	85.93	$309 \pm 3$	84.53	$300 \pm 3$
118.00 <sup>a</sup>	86.67	$331 \pm 3$	85.25	$322 \pm 3$
120.00	88.12	$378 \pm 4$	86.70	$375 \pm 4$
122.00	89.60	$427 \pm 4$		
123.00			88.88	$444 \pm 4$
124.00 <sup>a</sup>	91.07	$468 \pm 5$	89.60	$464 \pm 5$
126.00			91.05	$505 \pm 5$

<sup>a</sup>Energies at which full angular distributions were measured.

112.0, 118.0, and 124.0 MeV for both the systems. For these measurements, the velocity filter was moved in an angular range from  $-4^\circ$  to  $+10^\circ$ , typically in  $1^\circ$  steps, giving measurements from  $-24^\circ$  to  $-10^\circ$  with the SSB detector. The differential cross sections  $d\sigma_{\text{ER}}/d\Omega$  were measured at  $\pm 2^\circ$  in small energy steps in the range 99.0–124.0 MeV, as shown in Table II. All the ER yields were normalized to the elastic scattering yields in two monitor SSB detectors, mounted at  $\pm 30^\circ$  to the beam axis, where the elastic scattering was pure Rutherford. More details of the experimental method are given in Ref. [7].

Typical ER angular distributions obtained for the two reactions, at  $E_{\text{beam}} = 124.0$  MeV, are shown in Fig. 2. Each ER angular distribution was fitted using the sum of two Gaussian functions, indicated in the figure by solid lines; the dashed lines represent the component Gaussians. The difference in

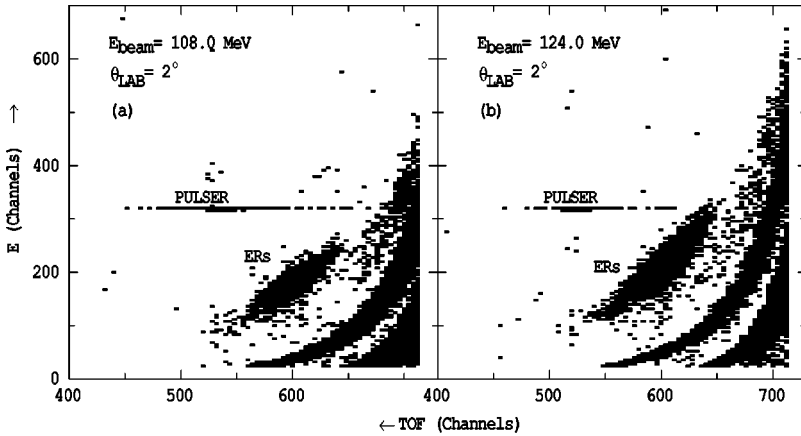


FIG. 1. Spectra of the energy  $E$ , measured in the position-sensitive surface barrier detector versus the time of flight using the MWPC for the reaction  $^{32}\text{S} + ^{89}\text{Y}$  at  $E_{\text{beam}} = 108.0$  and  $124.0$  MeV, showing the clear separation of ERs. Signals from the pulser used to measure dead-time are indicated. The bands of events on the right hand side of the spectra are from beam particles scattered upstream of the target.

shape of the two angular distributions is expected because of the higher probability for charged particle evaporation from the more neutron deficient compound nucleus formed in the  $^{32}\text{S}$ -induced reaction. As can be seen from Fig. 2 the experimental angular distributions deviate from the fits at the largest angles, which may be due to the evaporation of Li nuclei. Although, in principle, better fits to the angular distributions may be achieved, for example, by taking two Gaussians plus a Fermi-like function (a Gaussian function replaced by a flat region from  $0^\circ$  up to a certain angle, followed by a half Gaussian function) [18], the contributions from these higher angles are so small that the total cross sections are not sig-

nificantly affected. The total ER cross sections  $\sigma_{\text{ER}}$ , at energies where full angular distributions were measured, were obtained by integrating  $d\sigma_{\text{ER}}/d\theta$ , determined by multiplying the Gaussian fits by  $2\pi \sin \theta$ , over all values of  $\theta$ . The ratio of  $\sigma_{\text{ER}}$  to  $d\sigma_{\text{ER}}/d\Omega$  at  $\pm 2^\circ$  was found to be a linear function of  $E_{\text{beam}}$ . This function was used to determine the total ER cross sections at the other energies, where  $d\sigma_{\text{ER}}/d\Omega$  was measured only at  $\pm 2^\circ$ , using the method described in Ref. [19]. The total fusion cross section  $\sigma_{\text{fus}}$  was taken to be equal to  $\sigma_{\text{ER}}$  as fission is expected to be negligible in the energy range of the present measurements.

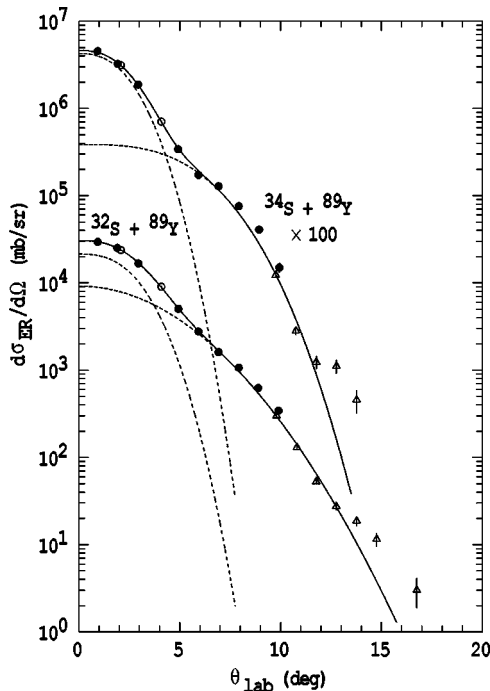


FIG. 2. Angular distributions of ERs for the two reactions,  $^{32,34}\text{S} + ^{89}\text{Y}$ , at  $E_{\text{beam}} = 124.0$  MeV. The solid lines are the sum of two Gaussian functions used to obtain the total cross sections. The component Gaussian functions are shown by the dashed lines. The filled and open circles are measurements using the velocity filter on opposite sides of the beam axis at positive and negative angles, respectively. The triangles are measured directly with the large solid angle SSB detector.

### III. RESULTS AND ANALYSIS

The resulting fusion excitation functions as a function of center-of-mass energy  $E_{\text{c.m.}}$  are plotted in Figs. 3(a) and 3(c). The  $E_{\text{c.m.}}$  have been corrected for energy loss in the target. Error bars shown correspond to 1% uncertainties [7], unless the uncertainties due to counting statistics were larger, in which case the latter were used. The experimental fusion barrier distributions were extracted [6] from the excitation functions for the two systems by evaluating the second derivative of the product of the cross section and the center-of-mass energy, denoted by  $d^2(E\sigma_{\text{fus}})/dE^2$ . In practice this was determined using a point difference formula [7], and the results are shown in Figs. 3(b) and 3(d). Energy step lengths  $\Delta E_{\text{c.m.}}$  in the range 2.0–2.5 MeV were used in extracting the barrier distributions. As seen from Figs. 3(b) and 3(d), the barrier distributions for the two reactions have somewhat different shapes, visible most clearly in the heights of the peaks at  $\approx 76$  MeV. To obtain a better comparison of the two systems, the reduced cross sections and the reduced barrier distributions were determined by dividing both quantities by  $\pi R_b^2$ , where  $R_b$  is the uncoupled barrier radius. These are plotted in Fig. 4 as a function of  $E_{\text{c.m.}}/V_b$ , where  $V_b$  is the average fusion barrier energy. The parameters  $R_b$  and  $V_b$  were determined as described later, and are given in Table III. The sub-barrier fusion cross sections for  $^{32}\text{S} + ^{89}\text{Y}$  are seen to be larger than those of  $^{34}\text{S} + ^{89}\text{Y}$ , and the shapes of the barrier distributions are also different. These differences are similar to those seen between the two reactions  $^{16}\text{O} + ^{144}\text{Sm}$  and  $^{17}\text{O} + ^{144}\text{Sm}$ , which were attributed to coupling to a neutron transfer channel with positive  $Q$  value for the

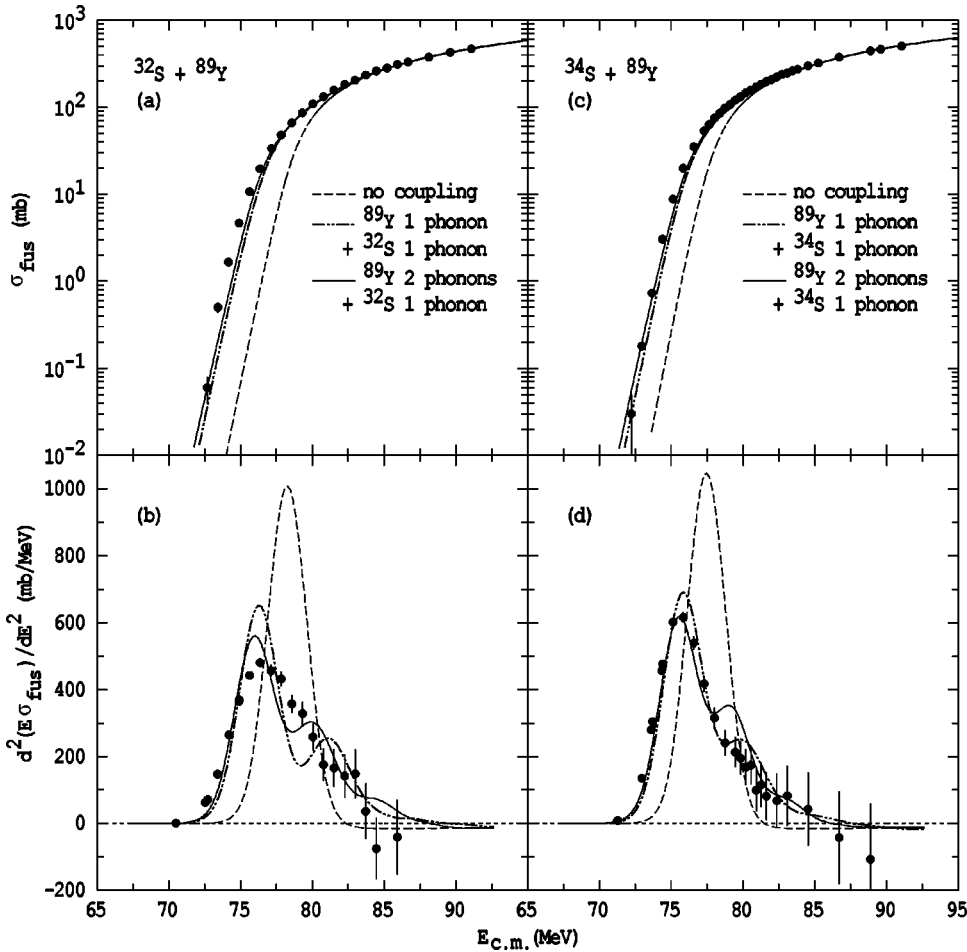


FIG. 3. Excitation functions [(a) and (c)] and barrier distributions [(b) and (d)] for the systems  $^{32,34}\text{S} + ^{89}\text{Y}$ . The dashed curves show the single barrier penetration calculations. Results of the exact coupled channels calculations including single-phonon states in  $^{32}\text{S}$  and single-phonon (dot-dot-dashed lines) and double-phonon states (solid lines) in  $^{89}\text{Y}$  are shown.

$^{17}\text{O}$  induced reaction [8]. Thus the difference in  $^{32}\text{S}$  and  $^{34}\text{S}$  reactions may be due to differences in their  $Q_{\text{eff}}$  values for proton transfer.

To investigate whether this is indeed the case for the reactions  $^{32,34}\text{S} + ^{89}\text{Y}$ , coupled channels calculations were performed. Because of the high energies of the excited states of the projectiles, it is important that interpretation of the data is carried out in the framework of a realistic coupled channels formalism, and for this reason the code CCFULL [20] was used. These calculations require an initial set of potential parameters. They were obtained from single-barrier penetration model fits to the cross sections well above the average fusion barrier, which are fairly insensitive to the form or magnitude of the couplings. The nuclear potential was taken to be of the Woods-Saxon form,

$$V_n(r) = -V_0 / \{1 + \exp[(r - r_0 A_P^{1/3} - r_0 A_T^{1/3})/a]\}, \quad (1)$$

where  $V_0$  is the depth,  $r_0$  is the radius parameter, and  $a$  is the diffuseness of the nuclear potential. The potential parameters were obtained by fixing  $r_0$  to 1.01 fm, and varying  $a$  and  $V_0$  to obtain a good fit to the high energy part of the cross sections. The parameters thus obtained, together with the uncoupled fusion barrier parameters derived from them, are listed in Table III. The CCFULL calculations in the no-coupling limit are shown by the dashed curves in Fig. 3.

While determining the barrier distributions from the theoretical cross sections, a constant energy step length of  $\Delta E_{\text{c.m.}} = 2.25$  MeV was used.

The first set of coupled channels calculations was performed including only one-phonon coupling to the vibrational states listed in Table IV. The target nucleus has an unpaired  $p_{1/2}$  proton that will couple with the  $2^+$  and  $3^-$  collective excitations (present in the neighboring even-even nuclei) to form a multiplet of states. To remain within the model space of CCFULL, the excitation energies and deformation parameters for  $^{89}\text{Y}$  were taken to be the averages of the corresponding values for the neighboring even-even nuclei  $^{88}\text{Sr}$  and  $^{90}\text{Zr}$ . Although this treatment is approximate, our conclusions in this paper arise from the differences seen in the fusion of the  $^{32}\text{S}$  and  $^{34}\text{S}$  projectiles, with the  $^{89}\text{Y}$  target nucleus being common. The inclusion of couplings in CCFULL shifts the average barrier position, and hence  $r_0$  was adjusted slightly to fit the high energy cross sections after the inclusion of each set of couplings. The dot-dot-dashed lines in Fig. 3 show the results of these one-phonon calculations. The solid lines indicate the results where, in addition, the double octupole phonon excitation of  $^{89}\text{Y}$  was included, in the harmonic limit. Thus the average energy of the double octupole phonon multiplet of  $^{89}\text{Y}$  was taken to be twice that of the single octupole phonon state, with the strength of coupling between the single- and double-phonon states being

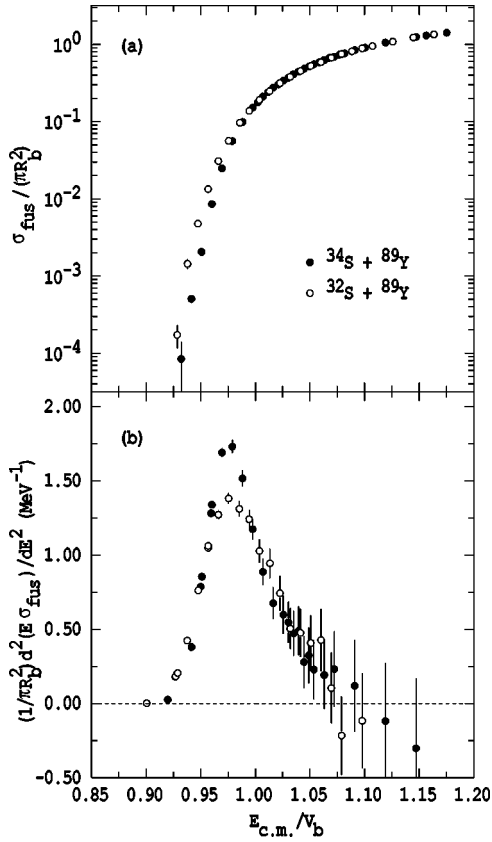


FIG. 4. Reduced excitation functions (a) and barrier distributions (b) for  $^{32,34}\text{S} + ^{89}\text{Y}$ .

given by  $\sqrt{2}\beta_3$ . Such double octupole phonon excitations were also required to explain fusion data for reactions involving the neighboring nucleus  $^{92}\text{Zr}$  [18]. The effects of including double-phonon quadrupole couplings in  $^{89}\text{Y}$  were found to be very small. All possible mutual excitations were included in all the above calculations.

For the reaction  $^{34}\text{S} + ^{89}\text{Y}$ , inclusion of double octupole phonon coupling in  $^{89}\text{Y}$  gives a good reproduction of the excitation function and a reasonable reproduction of the shape of the barrier distribution, as shown by the solid lines in Figs. 3(c) and 3(d). However, the corresponding calculations for  $^{32}\text{S} + ^{89}\text{Y}$ , shown in Figs. 3(a) and 3(b), give a good representation neither of the excitation function nor of the barrier distribution.

The effect of including coupling to proton transfer was therefore investigated. Since CCFULL does not treat the coupling to transfer channels exactly, only the qualitative effect

TABLE III. The potential parameters obtained from fitting the high energy fusion cross sections with  $r_0$  fixed at 1.01 fm. Also shown are the derived uncoupled barrier heights  $V_b$ , radii  $R_b$ , and curvatures  $\hbar\omega$ .

System	$V_0$ (MeV)	$r_0$ (fm)	$a$ (fm)	$V_b$ (MeV)	$R_b$ (fm)	$\hbar\omega$ (MeV)
$^{32}\text{S} + ^{89}\text{Y}$	201	1.01	0.85	78.28	10.52	3.60
$^{34}\text{S} + ^{89}\text{Y}$	209	1.01	0.85	77.48	10.64	3.49

TABLE IV. Excitation energies  $E_x$ , multiplicities  $\lambda$ , and deformation parameters  $\beta_\lambda$  [21,22] for the single-phonon vibrational states of the projectile and target used in the coupled channels calculations detailed in the text. The excitation energies and deformation parameters for  $^{89}\text{Y}$  were obtained by averaging the corresponding values for the neighboring even-even nuclei  $^{88}\text{Sr}$  and  $^{90}\text{Zr}$ .

Nucleus	$\lambda$	$E_x$ (MeV)	$\beta_\lambda$
$^{32}\text{S}$	2	2.230	0.312
$^{34}\text{S}$	2	2.128	0.252
$^{89}\text{Y}$	2	2.011	0.104
$^{89}\text{Y}$	3	2.742	0.208

of transfer on the fusion process can be studied in the framework of this code. Keeping this in mind, calculations were performed including one proton stripping channels in  $^{32,34}\text{S} + ^{89}\text{Y}$ . The one nucleon transfer form factor is normally taken to have an exponential form [23]. However, this form is valid only at distances  $r \geq R_b$  and cannot be used in CCFULL where the coupled channels equations need to be solved numerically also at distances  $r < R_b$ , and the code runs into a numerical difficulty. Instead a form factor  $F_{tran}(r)$ , which is proportional to the first derivative of the nuclear potential  $V_n(r)$  was used. Here  $F_{tran}(r)$  is given by

$$F_{tran}(r) = -F_{tr} \frac{dV_n(r)}{dr}, \quad (2)$$

where  $F_{tr}$  is the transfer coupling strength. This form factor has often been used for pair nucleon transfer [24]. Using the simplified coupled channels code CCMOD [25], it was checked that the two different form factors provided similar results as long as  $F_{tran}(r)$  was the same at  $r = R_b$ . The dashed lines in Figs. 5(a) and 5(b) show the results for  $^{34}\text{S} + ^{89}\text{Y}$ . The coupling to the one proton transfer channel with  $F_{tr} = 0.10$  fm was included, in addition to the inelastic excitations described above. This value of  $F_{tr}$  was chosen to give a good fit to the low energy cross sections and a reasonable fit was obtained for the barrier distribution. On the other hand, for  $^{32}\text{S} + ^{89}\text{Y}$ , with  $F_{tr} = 0.20$  fm, though an improved fit to the low energy cross sections could be achieved, the shape of the measured barrier distribution could not be reproduced. The results of these calculations are shown by the dashed lines in Figs. 6(a) and 6(b). Increasing the strength of  $F_{tr}$  and/or including the two proton transfer channel (with  $Q_{eff} = +3.90$  MeV), has little effect on the shape of the barrier distribution. Since the  $^{89}\text{Y}$  target nucleus is common to both reactions the difference in the cross sections and barrier distributions could be due to the different structure of the  $^{32}\text{S}$  and  $^{34}\text{S}$  projectiles.

The calculations presented so far have only included coupling to the  $2_1^+$  state of the projectile. In general, it is expected that there will be coupling from the first excited state to higher-lying states. Thus exclusion of couplings beyond the  $2_1^+$  state is reasonable only when the coupling to the  $2_1^+$  state is weak, and thus has little effect on the barrier distri-

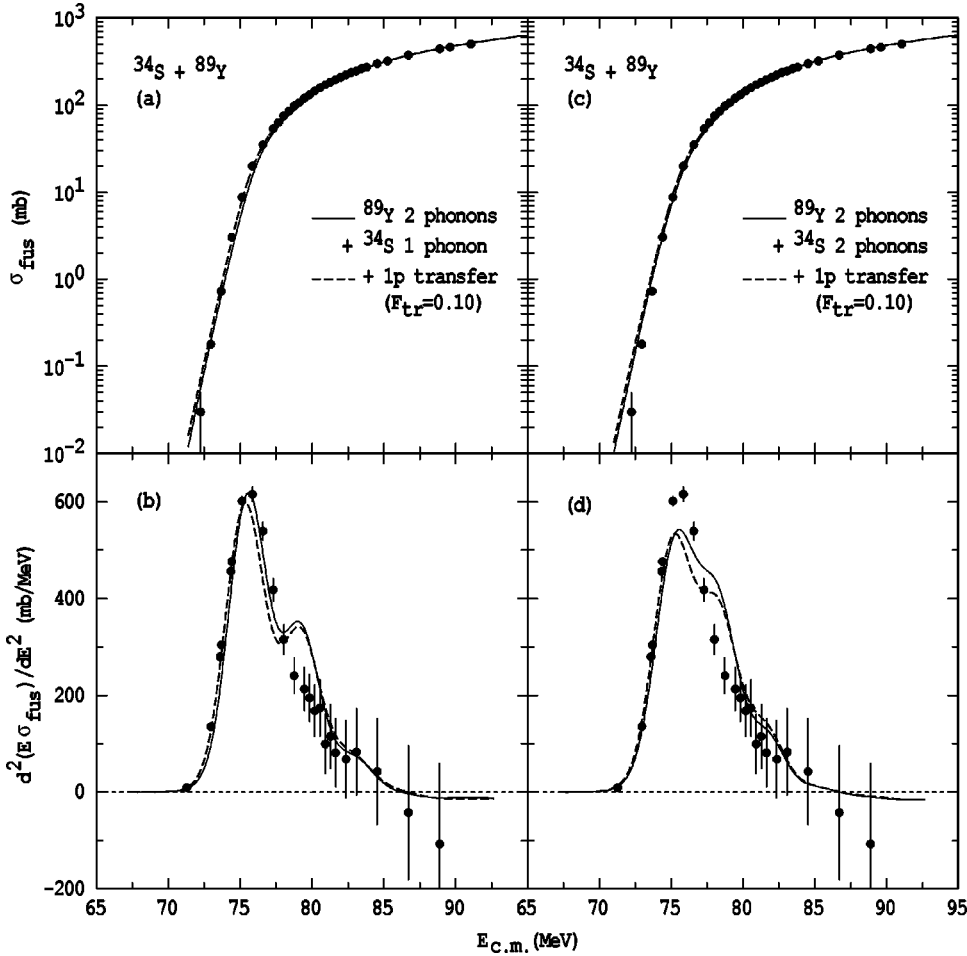


FIG. 5. Excitation function [(a) and (c)] and barrier distribution [(b) and (d)] for  $^{34}\text{S}+^{89}\text{Y}$  compared with exact coupled channels calculations performed with the code CCFULL. The calculations show the effects of coupling to proton transfer and inclusion of double quadrupole phonon states in  $^{34}\text{S}$ .

butions. This is not the case here, and hence couplings from the  $2_1^+$  state to higher states should be considered.

As discussed in Sec. I, features of the low-lying excited states of  $^{32}\text{S}$  suggest a vibrational character for this nucleus, whereas  $^{34}\text{S}$  is less collective, with smaller  $E2$  transition strengths. It was also argued that these two light nuclei are unlikely to behave as harmonic vibrators. However, not all parameters are known to allow a realistic anharmonic vibrator calculation to be performed. Thus the double-phonon calculations presented below were done in the harmonic limit, and hence represent the the upper limit of the couplings from the  $2_1^+$  states to higher-lying states in the projectiles. Taking couplings in  $^{89}\text{Y}$  to comprise of one quadrupole phonon and two octupole phonons in the harmonic limit, and with the inclusion of two quadrupole phonon ( $2^+ \otimes 2^+$ ) states in the projectiles, transfer coupling strengths of  $F_{tr}=0.10$  ( $^{34}\text{S}$ ) and  $F_{tr}=0.15$  ( $^{32}\text{S}$ ) best reproduced the low energy cross sections. These calculations are shown by the dashed lines in the right panels of Figs. 5 and 6. For comparison, equivalent calculations not including transfer are shown by the solid lines. Figures 5(c) and 5(d) show that for  $^{34}\text{S}+^{89}\text{Y}$ , inclusion of the  $2^+ \otimes 2^+$  excitation in  $^{34}\text{S}$  worsens the fit, apparent especially in the barrier distribution. Figures 6(c) and 6(d) show that inclusion of the  $2^+ \otimes 2^+$  excitation in  $^{32}\text{S}$  improves the agreement with the measured excitation function and the barrier distribution. In neither case is the harmonic limit expected to be appropriate, but it seems from the fusion

data that the coupling from the  $2_1^+$  state is stronger for  $^{32}\text{S}$  than for  $^{34}\text{S}$ , and is closer to the harmonic limit, consistent with a stronger vibrational character for  $^{32}\text{S}$ . Comparing the calculations in Figs. 5 and 6, we see that inclusion of the  $2^+ \otimes 2^+$  excitation has a much stronger effect than inclusion of the one proton transfer channel. This indicates that the influence of proton transfer on fusion is small in these reactions, and such dominance of collective couplings is consistent with previous conclusions [7,26]. Hence, the effects of collective couplings should be correctly incorporated prior to drawing any conclusion about the effect of nucleon transfer on the fusion barrier distributions.

#### IV. SUMMARY

Fusion cross sections have been measured to high precision at energies around the fusion barrier for  $^{32,34}\text{S}+^{89}\text{Y}$ , and the fusion barrier distributions have been extracted from the data. These measurements were initially performed to investigate the sensitivity of fusion to proton transfer channels with positive effective  $Q$  values. The values of  $Q_{\text{eff}}$  for one- and two-proton stripping channels are more positive for  $^{32}\text{S}+^{89}\text{Y}$  compared to  $^{34}\text{S}+^{89}\text{Y}$ . The sub-barrier fusion cross sections for  $^{32}\text{S}+^{89}\text{Y}$  are larger than those of  $^{34}\text{S}+^{89}\text{Y}$ , and the shapes of the experimental barrier distributions are significantly different. The data have been interpreted using the realistic coupled channels code CCFULL. The

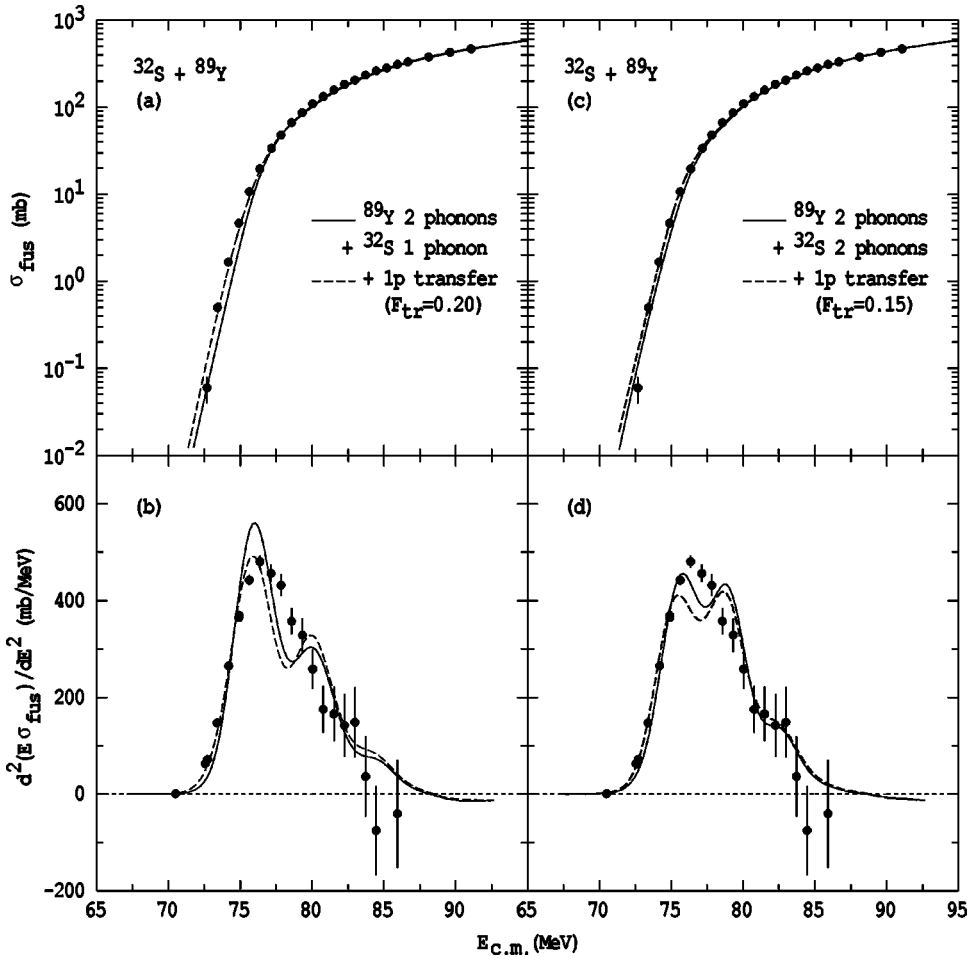


FIG. 6. Excitation function [(a) and (c)] and barrier distribution [(b) and (d)] for  $^{32}\text{S}+^{89}\text{Y}$  compared with exact coupled channels calculations performed with the code CCFULL. The calculations show the effects of coupling to proton transfer and inclusion of double quadrupole phonon states in  $^{32}\text{S}$ .

low energy cross sections are the most sensitive to couplings to positive  $Q$ -value transfer channels. The inclusion of couplings to proton stripping channels gives improved fits to the low energy cross sections, but does not explain the differences in the cross sections for the two systems at energies around the average barriers, which are seen most clearly in the barrier distributions. Since the  $^{89}\text{Y}$  target nucleus is common to both reactions, the difference in the experimental results must arise from the difference in the structure of the projectiles. The data were best reproduced by including one quadrupole phonon excitation in  $^{34}\text{S}$ , and two-phonon excitation in  $^{32}\text{S}$ . This is consistent with the spectroscopic evi-

dence that indicates a stronger vibrational character for  $^{32}\text{S}$  than for  $^{34}\text{S}$ . It is concluded that the difference between the two systems lies mainly in the collectivity of the projectiles, whilst the effect of proton transfer on the fusion process is small in these reactions.

#### ACKNOWLEDGMENTS

We would like to thank B. R. Barrett for useful discussions. M.D. acknowledges financial support from the Australian Research Council.

- 
- [1] S.G. Steadman and M.J. Rhoades-Brown, *Annu. Rev. Nucl. Part. Sci.* **36**, 649 (1986), and references therein.
- [2] M. Beckerman, *Rep. Prog. Phys.* **51**, 1047 (1988), and references therein.
- [3] W. Reisdorf, *J. Phys. G* **20**, 1297 (1994).
- [4] M. Dasgupta, D.J. Hinde, N. Rowley, and A.M. Stefanini, *Annu. Rev. Nucl. Part. Sci.* **48**, 401 (1998), and references therein.
- [5] C.H. Dasso, S. Landowne, and A. Winther, *Nucl. Phys.* **A405**, 381 (1982); **A407**, 221 (1983).
- [6] N. Rowley, G.R. Satchler, and P.H. Stelson, *Phys. Lett. B* **254**, 25 (1991).
- [7] J.R. Leigh, M. Dasgupta, D.J. Hinde, J.C. Mein, C.R. Morton, R.C. Lemmon, J.P. Lestone, J.O. Newton, H. Timmers, J.X. Wei, and N. Rowley, *Phys. Rev. C* **52**, 3151 (1995).
- [8] C.R. Morton, M. Dasgupta, D.J. Hinde, J.R. Leigh, R.C. Lemmon, J.P. Lestone, J.C. Mein, J.O. Newton, H. Timmers, N. Rowley, and A.T. Kruppa, *Phys. Rev. Lett.* **72**, 4074 (1994).
- [9] A.M. Stefanini, D. Ackermann, L. Corradi, J.H. He, G. Mon-

- tagnoli, S. Beghini, F. Scarlassara, and G.F. Segato, *Phys. Rev. C* **52**, R1727 (1995).
- [10] H. Timmers, D. Ackermann, S. Beghini, L. Corradi, J.H. He, G. Montagnoli, F. Scarlassara, A.M. Stefanini, and N. Rowley, *Nucl. Phys.* **A633**, 421 (1998).
- [11] A.A. Sonzogni, J.D. Bierman, M.P. Kelly, J.P. Lestone, J.F. Liang, and R. Vandenbosch, *Phys. Rev. C* **57**, 722 (1998).
- [12] R.A. Broglia, C.H. Dasso, and S. Landowne, *Phys. Rev. C* **32**, 1426 (1985).
- [13] K.E. Rehm, H. Esbensen, C.L. Jiang, B.B. Back, F. Borasi, B. Harss, R.V.F. Janssens, V. Nanal, J. Nolen, R.C. Pardo, M. Paul, P. Reiter, R.E. Segel, A. Sonzogni, J. Uusitalo, and A.H. Wuosmaa, *Phys. Rev. Lett.* **81**, 3341 (1998).
- [14] A. Kangasmäki, P. Tikkamen, J. Keinonen, W.E. Ormand, S. Raman, Zs. Fülöp, Á.Z. Kiss, and E. Somorjai, *Phys. Rev. C* **58**, 699 (1998).
- [15] M.W. Greene, P.R. Alderson, D.C. Bailey, J.L. Durell, L.L. Green, A.N. James, and J.F. Sharpey-Schafer, *Nucl. Phys.* **A148**, 351 (1970).
- [16] P. Raghavan, *At. Data Nucl. Data Tables* **42**, 189 (1989).
- [17] J.X. Wei, J.R. Leigh, D.C. Weissler, J.O. Newton, S. Elfström, J.P. Lestone, J.X. Chen, D.G. Popescu, and D.J. Hinde, *Nucl. Instrum. Methods Phys. Res. A* **306**, 557 (1991).
- [18] J.O. Newton, C.R. Morton, M. Dasgupta, J.R. Leigh, J.C. Mein, D.J. Hinde, H. Timmers, and K. Hagino, *Phys. Rev. C* **64**, 064608 (2001).
- [19] J.X. Wei, J.R. Leigh, D.J. Hinde, J.O. Newton, R.C. Lemmon, S. Elfström, J.X. Chen, and N. Rowley, *Phys. Rev. Lett.* **67**, 3368 (1991).
- [20] K. Hagino, N. Rowley, and A.T. Kruppa, *Comput. Phys. Commun.* **123**, 143 (1999).
- [21] S. Raman, C.H. Malarkey, W.T. Milner, C.W. Nestor, and P.H. Stelson, *At. Data Nucl. Data Tables* **36**, 1 (1987).
- [22] R.H. Spear, *At. Data Nucl. Data Tables* **42**, 55 (1989).
- [23] R.A. Broglia, G. Pollarolo, and A. Winther, *Nucl. Phys.* **A406**, 369 (1983).
- [24] C.H. Dasso and G. Pollarolo, *Phys. Lett.* **155B**, 223 (1985); C.H. Dasso and A. Vitturi, *Phys. Lett. B* **179**, 337 (1986).
- [25] M. Dasgupta, A. Navin, Y.K. Agarwal, C.V.K. Baba, H.C. Jain, M.L. Jhingan, and A. Roy, *Nucl. Phys.* **A539**, 351 (1992).
- [26] R.A. Broglia, C.H. Dasso, S. Landowne, and G. Pollarolo, *Phys. Lett.* **133B**, 34 (1983).